Causality of holographic hydrodynamics

JHEP08(2009)016

(http://iopscience.iop.org/1126-6708/2009/08/016)

Published by IOP Publishing for SISSA

Received: *June 29, 2009*
Revised: *July 18, 2009*
Accepted: *July 23, 2009*
Published: *August 6, 2009*

Causality of holographic hydrodynamics

Alex Buchel[a,b] **and Robert C. Myers**[a]

[a] *Perimeter Institute for Theoretical Physics, Waterloo, Ontario N2L 2Y5, Canada*
[b] *Department of Applied Mathematics, University of Western Ontario, London, Ontario N6A 5B7, Canada*

E-mail: abuchel@perimeterinstitute.ca, rmyers@perimeterinstitute.ca

Abstract: We study causality violation in holographic hydrodynamics in the gauge theory/string theory correspondence, focussing on Gauss-Bonnet gravity. The value of the Gauss-Bonnet coupling is related to the difference between the central charges of the dual conformal gauge theory. We show that, when this difference is sufficiently large, causality is violated both in the second-order truncated theory of hydrodynamics, as well as in the exact theory. We find that the latter provides more stringent constraints, which match precisely those appearing in the CFT analysis of Hofman and Maldacena.

Keywords: Gauge-gravity correspondence, AdS-CFT Correspondence

ArXiv ePrint: 0906.2922

doi:10.1088/1126-6708/2009/08/016

Contents

JHEP08(2009)016

1 Introduction

Hydrodynamics organizes the description of the macroscopic evolution of systems in local, but not global, equilibrium in terms of a derivative expansion. For concreteness, we will consider a four-dimensional relativistic fluid here. In the simplest situation (with no conserved charges), the dynamics of the hydrodynamic fluctuations in the fluid is simply governed by conservation of the stress-energy tensor $T^{\mu\nu}$,

$$\nabla_\nu T^{\mu\nu} = 0\,. \tag{1.1}$$

The stress-energy tensor includes both an equilibrium part (with local energy density ε and pressure P) and a dissipative part $\Pi^{\mu\nu}$,

$$T^{\mu\nu} = \varepsilon\, u^\mu u^\nu + P\Delta^{\mu\nu} + \Pi^{\mu\nu} \quad \text{where} \quad \Delta^{\mu\nu} = g^{\mu\nu} + u^\mu u^\nu\,. \tag{1.2}$$

Above, u^μ is the local four-velocity of the fluid with $u^\mu u_\mu = -1$. Further, $\Pi^{\mu\nu}u_\nu = 0$. In phenomenological hydrodynamics, the dissipative term $\Pi^{\mu\nu}$ can be represented as an infinite series expansion in velocity gradients (and curvatures, for a fluid in a curved background), with the coefficients of the expansion commonly referred to as transport coefficients. The familiar example of the Navier-Stokes equations are obtained by truncating $\Pi^{\mu\nu}$ at linear order in this expansion

$$\Pi^{\mu\nu} = \Pi_1^{\mu\nu}(\eta,\zeta) = -\eta\,\sigma^{\mu\nu} - \zeta\,\Delta^{\mu\nu}\,\nabla\cdot u\,, \tag{1.3}$$

where

$$\sigma^{\mu\nu} = 2\nabla^{\langle\mu}u^{\nu\rangle} \equiv \Delta^{\mu\alpha}\Delta^{\nu\beta}\left(\nabla_\alpha u_\beta + \nabla_\beta u_\alpha\right) - \frac{2}{3}\Delta^{\mu\nu}\left(\Delta^{\alpha\beta}\nabla_\alpha u_\beta\right)\,. \tag{1.4}$$

Notice that at this order in the hydrodynamic approximation we need to introduce only two transport coefficients, namely the shear η and bulk ζ viscosities. In the following discussion, we will be particularly interested in describing conformal fluids, in which case we must also impose the vanishing of the trace of the stress tensor. This restriction fixes $\zeta = 0$, as well as $P = \varepsilon/3$ in the equilibrium contribution.

As noted above, hydrodynamics can be regarded as giving a systematic derivative expansion. Within this framework, it is then straightforward to extend $\Pi^{\mu\nu}$ to the next order to including terms of order $\nabla^2 u$ or $(\nabla u)^2$. In general, this extension would require the introduction thirteen new transport coefficients [1]. However, if we again restrict our attention of conformal fluids, the second-order term Π_2 only depends on five of these new transport coefficients [2]. While the interested reader can find the complete description in [2], we only illustrate the extension here by showing the first few new terms:

$$\begin{aligned}\Pi^{\mu\nu} &= \Pi_1^{\mu\nu}(\eta) + \Pi_2^{\mu\nu}\left(\eta, \tau_\Pi, \kappa, \lambda_1, \lambda_2, \lambda_3\right) \\ &= -\eta\,\sigma^{\mu\nu} - \eta\,\tau_\Pi\left[{}^{\langle}u\cdot\nabla\sigma^{\mu\nu\rangle} + \frac{1}{3}\,(\nabla\cdot u)\;\sigma^{\mu\nu}\right] + \lambda_1\,\sigma^{\langle\mu}{}_{\alpha}\,\sigma^{\nu\rangle\alpha} + \cdots\,.\end{aligned} \tag{1.5}$$

The terms controlled by $\lambda_{2,3}$ involve the vorticity while κ term is proportional to the spacetime curvature. Hence the terms explicitly given above are sufficient to describe the vorticity-free flow of a conformal fluid in a flat background spacetime. As noted in [2], the first term proportional to τ_Π essentially captures the second-order formalism of Müller, Israel and Stewart (MIS) [3] while the subsequent nonlinear terms already represent an extension of their approach. However, this linear term is sufficient to address the question of causality within the hydrodynamic framework. It is well known that if the dissipative contribution is truncated as in (1.3), for any viscosity coefficients $\{\eta, \zeta\}$, there are always linearized fluctuations for which the wave-front speed is superluminal [4]. The primary motivation of MIS was then to eliminate this acausality in the hydrodynamic equations. Indeed the MIS term is sufficient to tame the superluminal propagation with an appropriate choice of the relaxation time τ_Π, as we demonstrate below [5]. However, we add that, as will become evident, the constraints on τ_Π emerge from the behaviour of modes outside the regime of validity of the second-order hydrodynamic framework, i.e., from very short wavelength modes. Hence, one should keep in mind that these constraints do not signal any fundamental pathologies but rather only indicate where a certain approximate mathematical framework describing the fluid becomes problematic. Nevertheless, a causal system of second-order hydrodynamic equations is still required in many situations, such as, numerical simulations [6] which implicitly extrapolate the hydrodynamic equations to the smallest numerical scales, even though the physics of interest is in the long wavelength regime.

Linearized fluctuations of the second-order truncated hydrodynamics in conformal fluids were discussed in [2]:

- The dispersion relation of the shear channel fluctuations is given by (see eq. (3.27) of [2])

$$-\,\mathfrak{w}^2\;\tau_\Pi T - \frac{i\mathfrak{w}}{2\pi} + \boldsymbol{k}^2\;\frac{\eta}{s} = 0\,, \tag{1.6}$$

JHEP08(2009)016

where $\mathfrak{w} = \omega/(2\pi T)$ and $\boldsymbol{k} = k/(2\pi T)$. Now the speed with which a wave-front propagates out from a discontinuity in any initial data is governed by [7]

$$\lim_{|\boldsymbol{k}|\to\infty} \left.\frac{\mathrm{Re}\,(\mathfrak{w})}{\boldsymbol{k}}\right|_{[\mathrm{shear}]} = \sqrt{\frac{\eta}{s\ \tau_\Pi T}} \equiv v^{\mathrm{front}}_{[\mathrm{shear}]}\,. \tag{1.7}$$

Hence causality in this channel imposes the restriction

$$\tau_\Pi T \ \geq \frac{\eta}{s}\,. \tag{1.8}$$

- The dispersion relation of the sound channel fluctuations is given by (see eq. (3.20) of [2])

$$-\,\mathfrak{w}^3\tau_\Pi T - \frac{i\mathfrak{w}^2}{2\pi} + \frac{1}{3}\tau_\Pi T\ \mathfrak{w}\boldsymbol{k}^2 + \frac{4\eta}{3s}\ \mathfrak{w}\boldsymbol{k}^2 + \frac{i\boldsymbol{k}^2}{6\pi} = 0\,. \tag{1.9}$$

Hence

$$\lim_{|\boldsymbol{k}|\to\infty} \left.\frac{\mathrm{Re}\,(\mathfrak{w})}{\boldsymbol{k}}\right|_{[\mathrm{sound}]} = \sqrt{\frac{1}{3} + \frac{4\eta}{3s}\ \frac{1}{\tau_\Pi T}} \equiv v^{\mathrm{front}}_{[\mathrm{sound}]}\,. \tag{1.10}$$

From (1.10), causality in the sound channel imposes the following condition

$$\tau_\Pi T \ \geq 2\frac{\eta}{s}\,. \tag{1.11}$$

From (1.7) and (1.10) above, we might note that both $v^{\mathrm{front}}_{[\mathrm{shear}]}$ and $v^{\mathrm{front}}_{[\mathrm{sound}]}$ diverge as $\tau_\Pi \to 0$. We may also see that the front velocity in the sound channel is always larger than that in the shear channel[1] and hence the former provides a more stringent constraint (1.11) on the transport coefficients of the second-order hydrodynamics. Again, we note that as should be evident from (1.7) and (1.10), these restrictions arise from pushing the second-order hydrodynamic framework beyond its natural regime of validity, i.e., $|\boldsymbol{k}| \ll 1$. We return to this point in greater detail in section 4.

In principle, all the transport coefficients are determined by parameters of the underlying microscopic theory. In practice, such computations are prohibitively complicated as one has to *derive* the effective theory of hydrodynamics for a given microscopic system. The difficulties become even more insurmountable for strongly coupled plasmas, as might be of interest at RHIC (or the LHC). However, the AdS/CFT correspondence of Maldacena [9, 10] provides a new framework in which transport coefficients are readily calculable at least for certain strongly coupled gauge theories [2, 11, 12]. Furthermore, it is a context where the discussion of conformal fluids becomes particularly relevant. With reference to the constraints above, one has $\eta/s = 1/(4\pi)$ [13] and $\tau_\Pi T = (2 - \log 2)/(2\pi)$ [2, 11] for $N = 4$ super-Yang-Mills or any strongly coupled four-dimensional gauge theory for which the holographic dual is described by Einstein gravity [14]. Hence a second-order hydrodynamic analysis of such holographic plasmas does not suffer from any problems with acausality.[2]

[1] In fact, this is a general result which extends to nonconformal fluids as well [8].

[2] A full analysis of causality in these holographic plasmas was also discussed in [15].

JHEP08(2009)016

In this paper we extend this analysis using a particular effective model in the gauge theory/string theory correspondence. Specifically, we consider a holographic model with a Gauss-Bonnet (GB) gravity dual,

$$\mathcal{I} = \frac{1}{2\ell_P^3}\int d^5x\sqrt{-g}\left[\frac{12}{L^2} + R + \frac{\lambda_{\rm GB}}{2}L^2\left(R^2 - 4R_{\mu\nu}R^{\mu\nu} + R_{\mu\nu\rho\sigma}R^{\mu\nu\rho\sigma}\right)\right]. \tag{1.12}$$

The corresponding conformal gauge theory is distinguished by having two distinct central charges [16, 17] — see section 4 for details. The effect of such curvature-squared interactions on holographic hydrodynamics was examined in the context of string theory in [18], however, only within a perturbative framework. The GB gravity theory (1.12) is particularly well-behaved allowing the holographic analysis to be extended to finite values of the coupling $\lambda_{\rm GB}$. In particular, the ratio of the shear viscosity to the entropy density is found to be [19]

$$\frac{\eta}{s} = \frac{1}{4\pi}\Big[1 - 4\lambda_{\rm GB}\Big]. \tag{1.13}$$

Below we compute the relaxation time of the CFT plasma dual to GB gravity (1.12), $\tau_\Pi = \tau_\Pi(\lambda_{\rm GB})$. We find that the causality condition (1.11) then constrains $\lambda_{\rm GB}$ both from above and below. Note that in this case, the constraints are imposed to avoid fundamental inconsistencies in the theory. Further, these constraints on $\lambda_{\rm GB}$ would in turn lead to bounds on the viscosity in GB hydrodynamics.

The analysis of the second-order hydrodynamics in GB gravity is interesting because causality violations were already used to produce an upper bound on the GB coupling in [20]. The analysis there also examined the propagation of signals through the dual gauge theory plasma but made no restriction to second-order hydrodynamics. Hence we turn to the study of causality violation in an exact analysis of the GB theory in section 3. Following [21], the dispersion relation of physical fluctuations in a gauge theory plasma is identified with the dispersion relation of the quasinormal modes of a black hole in a dual gravitational description. Extending analysis of [20], we study dispersion relation of the GB BH quasinormal modes in the shear and the sound channels. As was done for the scalar channel in [20], we show that requiring that these modes are not superluminar, i.e., the phase velocity remains less than one in the infinite momentum limit, constraints $\lambda_{\rm GB}$. We find that combined these constraints are more stringent than the causality constraints coming from the second-order truncated GB hydrodynamics.

2 Causality of second-order Gauss-Bonnet hydrodynamics

We are interested in determining when the second-order hydrodynamics dual to GB gravity satisfies the causality constraint (1.11). Since the ratio of shear viscosity to entropy density is already given in (1.13), it only remains to determine the relaxation time τ_Π for the dual plasma. The simplest approach to discover $\tau_\Pi(\lambda_{\rm GB})$ is to examine the dispersion relation of the sound quasinormal mode of a GB black hole. Here, the field theory considerations establish that [2]:

$$\mathfrak{w} = c_s\boldsymbol{k} - 2\pi i\ \Gamma T\ \boldsymbol{k}^2 + \frac{4\pi^2\Gamma T}{c_s}\left(c_s^2\ \tau_\Pi T - \frac{1}{2}\Gamma T\right)\ \boldsymbol{k}^3 + \mathcal{O}(\boldsymbol{k}^4). \tag{2.1}$$

With

$$\Gamma T = \frac{2\eta}{3s} \quad \text{and} \quad c_s = \frac{1}{\sqrt{3}}\,, \tag{2.2}$$

this expression is simply the Taylor series solution of the dispersion relation (1.9).

In the dual gravitational description the dispersion relation (2.1) is obtained by imposing the incoming wave boundary condition at the horizon and the Dirichlet condition at the boundary on the sound channel quasinormal mode wavefunction. The technique is clearly explained in [21]. Here, we only present the salient steps in our analysis.[3]

The planar black hole solution in GB gravity can be written as [22, 23]

$$ds^2 = \frac{r_+^2}{u\,L^2}\left(-f(u)\mathcal{A}^2 dt^2 + \sum_{i=1}^{3} dx_i^2\right) + \frac{L^2}{f(u)}\frac{du^2}{4u^2}\,, \tag{2.3}$$

where

$$f(u) = \frac{1-\sqrt{1-4\lambda_{\rm GB}(1-u^2)}}{2\lambda_{\rm GB}}\,, \tag{2.4}$$

and

$$\mathcal{A}^2 = \frac{1}{2}\left(1+\sqrt{1-4\lambda_{\rm GB}}\right)\,. \tag{2.5}$$

The horizon is located at $u=1$ and asymptotic boundary is reached with $u\to 0$.[4] Note that the normalization constant $\mathcal{A}$ is chosen so that $\mathcal{A}^2\, f(u=0)=1$. Hence the asymptotic behaviour of the metric shows that the AdS curvature scale is $\mathcal{A}\,L$. The Hawking temperature, entropy density, and energy density of the black hole are

$$T = \mathcal{A}\,\frac{r_+}{\pi L^2}\,, \qquad s = \frac{1}{4G_N}\left(\frac{r_+}{L}\right)^3\,, \qquad \varepsilon = \frac{3}{4}Ts\,. \tag{2.6}$$

Now the sound channel quasinormal mode satisfies the following equation

$$Z''_{[\rm sound]}(u) + \mathcal{C}^{(1)}_{\rm sound}\; Z'_{[\rm sound]}(u) + \mathcal{C}^{(2)}_{\rm sound}\; Z_{[\rm sound]}(u) = 0\,, \tag{2.7}$$

where the coefficients $\mathcal{C}^{(i)}_{\rm sound}$ are presented in appendix A. In the hydrodynamic limit, $\boldsymbol{k}$, $\mathfrak{w}\to 0$ with $\frac{\mathfrak{w}}{\boldsymbol{k}}$ kept fixed, the incoming wave boundary condition at the horizon implies

$$Z_{[\rm sound]} = (1-u^2)^{-\frac{i\mathfrak{w}}{2}}\left(z_0(u;\mathfrak{w},\boldsymbol{k}) + i\boldsymbol{k}\; z_1(u;\mathfrak{w},\boldsymbol{k}) + \boldsymbol{k}^2\; z_2(u;\mathfrak{w},\boldsymbol{k}) + \mathcal{O}(\boldsymbol{k}^3)\right)\,, \tag{2.8}$$

with

$$\begin{aligned} &z_i(u;\mu\;\mathfrak{w},\mu\;\boldsymbol{k}) = z_i(u;\mathfrak{w},\boldsymbol{k})\,, \qquad \text{for any } \mu\,, \qquad i=0,1,2\\ &\lim_{u\to 1} z_i(u;\mathfrak{w},\boldsymbol{k}) = \delta_i^0\,. \end{aligned} \tag{2.9}$$

[3] Further computational details are available from the authors upon request.

[4] A more conventional radial coordinate [19, 22] would be given by $r^2 = r_+^2/u$. Implicitly we have also chosen the branch of well-behaved solutions and we are restricting our considerations to $\lambda_{\rm GB} < 1/4$ — see [22, 23] for details.

JHEP08(2009)016

In (2.8) we kept terms in the hydrodynamic expansion to the order necessary to identify (2.1). The sound wave dispersion relation (2.1) is then obtained by imposing the Dirichlet condition on $Z_{[\text{sound}]}$ at the boundary

$$\lim_{u\to 0} Z_{\text{sound}} = 0\,. \tag{2.10}$$

To leading order in the hydrodynamic approximation we find

$$z_0 = \frac{\boldsymbol{k}^2(x+4\lambda_{\text{GB}}-1)\mathcal{A}^2 - 6\lambda_{\text{GB}}\mathfrak{w}^2 x}{2\lambda_{\text{GB}}(2\mathcal{A}^2\boldsymbol{k}^2 - 3\mathfrak{w}^2)x}\,, \tag{2.11}$$

where we used a more convenient radial coordinate

$$x = \left(1 - 4\lambda_{\text{GB}} + 4\lambda_{\text{GB}}u^2\right)^{1/2}\,. \tag{2.12}$$

Imposing the Dirichlet condition (2.10) at this order recovers the conformal sound speed: $c_s = 1/\sqrt{3}$.

To order $\mathcal{O}(\boldsymbol{k})$ in (2.8), we find

$$\begin{aligned} z_1 =& \frac{\mathfrak{w}}{8\boldsymbol{k}}\left(\lambda_{\text{GB}}(2\mathcal{A}^2\boldsymbol{k}^2 - 3\mathfrak{w}^2)\ x\right)^{-1} \times \left(2(\mathcal{A}^2\boldsymbol{k}^2(x+4\lambda_{\text{GB}}-1) - 6\mathfrak{w}^2\lambda_{\text{GB}}x)\ \ln\frac{1+x}{2}\right. \\ &\left. + (1-x)\mathcal{A}^2\boldsymbol{k}^2(x^2 - 6x + 36\lambda_{\text{GB}}x + 12\lambda_{\text{GB}} - 3) + 6\mathfrak{w}^2\lambda_{\text{GB}}x(x+3)(x-1)\right)\,. \end{aligned} \tag{2.13}$$

Imposing the Dirichlet condition (2.10) at order $\mathcal{O}(\boldsymbol{k}^2)$ identifies

$$\frac{\eta}{s} = \frac{1}{4\pi}\left[1 - 4\lambda_{\text{GB}}\right]\,, \tag{2.14}$$

in precise agreement with the result (1.13) which was originally determined with a Kubo formula computation in [19].

Unfortunately, we were not able to evaluate z_2 (and as a result τ_Π) analytically. Thus, we had to resort to numerical analysis. For the question of causality, we are not interested here in τ_Π per se, but rather in the relation (1.11). Hence figure 1 presents the difference $\left(\tau_\Pi T - 2\frac{\eta}{s}\right)$ as a function of λ_{GB}. We find that unless $\lambda_{\text{GB}} \in [\lambda_{\text{min}}, \lambda_{\text{max}}]$, where $\lambda_{\text{min}} = -0.711(2)$ and $\lambda_{\text{max}} = 0.113(0)$, causality of the second-order truncated hydrodynamics of the GB plasma is violated. In figure 2, we also present the front velocities in the shear (1.7) and sound (1.10) channels. Note that we find that the relaxation time vanishes for $\lambda_{\text{GB}} = 0.165(5)$, which causes both of the front velocities to diverge at this point in the figure. The graph also demonstrates that $v^{\text{front}}_{[shear]} < v^{\text{front}}_{[sound]}$, as noted above.

3 Causality of full Gauss-Bonnet theory

In the previous section we showed that depending on the value of a the GB coupling, λ_{GB}, or equivalently on the values of the microscopic parameters in the dual CFT, causality of the second-order truncated hydrodynamics of the dual theory can be lost. In this section, we

JHEP08(2009)016

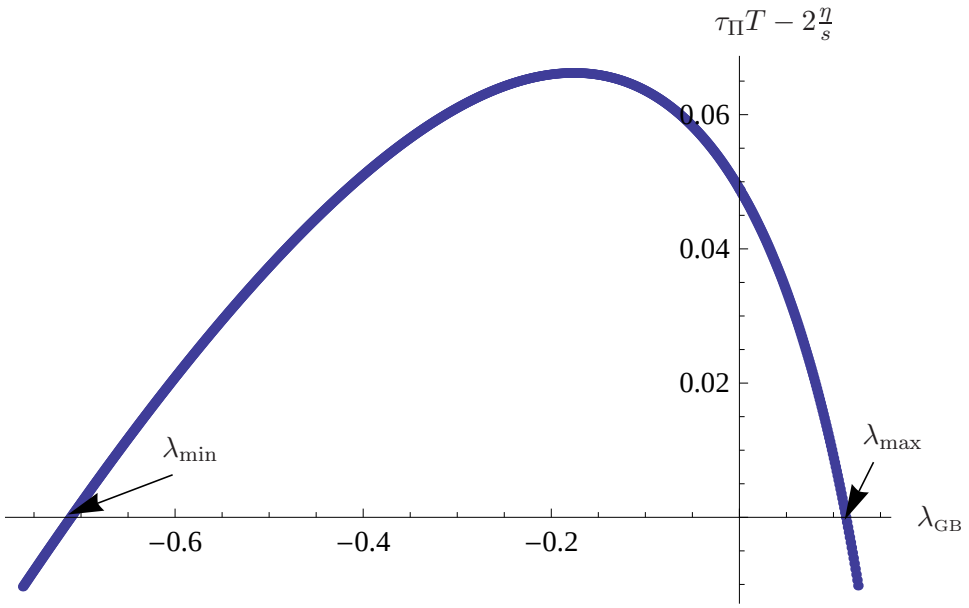

Figure 1. Causality of the second-order Gauss-Bonnet hydrodynamics is violated once $\tau_\Pi T < 2\frac{\eta}{s}$. Thus, $\lambda_{\rm GB} \in [\lambda_{\rm min}, \lambda_{\rm max}]$, where $\lambda_{\rm min} = -0.711(2)$ and $\lambda_{\rm max} = 0.113(0)$.

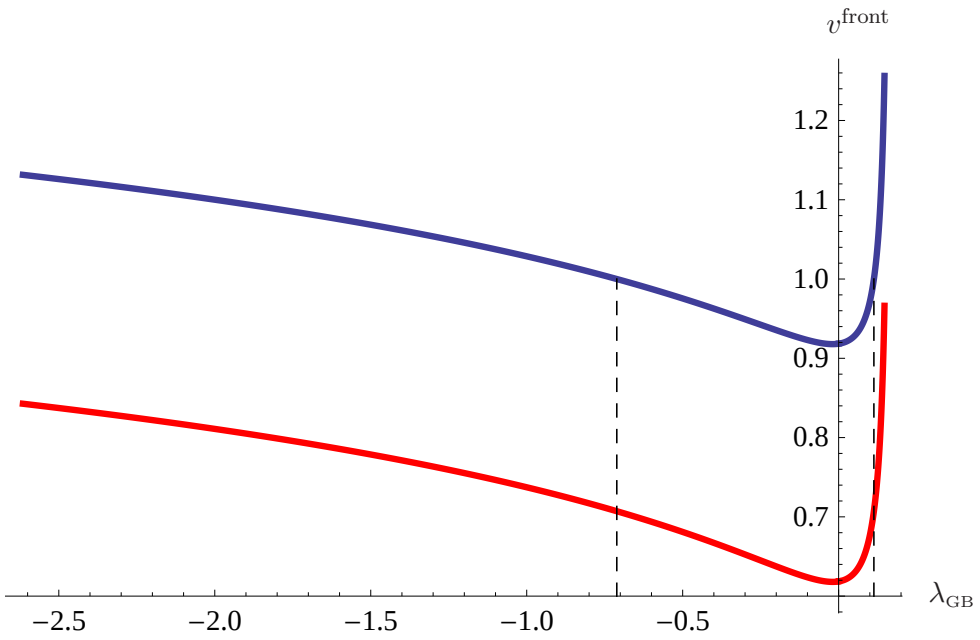

Figure 2. (Colour online) Front velocity for the shear (red) and sound (blue) channels for the second-order hydrodynamics, as given in (1.7) and (1.10). The dashed vertical lines indicate $\lambda_{\rm min}$ and $\lambda_{\rm max}$, where $v^{\rm front}_{[\rm sound]}$ reaches one.

wish to compare those results to causality violations found with the analysis of [20]. While the latter also looks for the appearance of superluminal signals propagating in the dual plasma, it makes no reference to truncating the derivative expansion in the hydrodynamic framework. We will find that the constraints on $\lambda_{\rm GB}$ arising from the exact analysis are

JHEP08(2009)016

more restrictive than those found in the truncated second-order hydrodynamic analysis in the previous section.

Dispersion relation of the linearized fluctuations in plasma is identified with the dispersion relation of the quasinormal modes of a black hole in the dual gravitational description. There are three types of quasinormal modes in gravitational geometries with translationary invariant horizons [21, 24]:

- a scalar channel (helicity-two graviton polarizations);
- a shear channel (helicity-one graviton polarizations);
- a sound channel (helicity-zero graviton polarizations).

While the shear and sound channels correspond to those considered in the previous discussion of second-order hydrodynamics, the scalar channel was not mentioned there because it contains no modes whose frequency vanishes as $\boldsymbol{k} \to 0$. Of course, this is in agreement with the standard hydrodynamic analysis [4]. However, the scalar channel quasinormal modes of the GB black holes in the limit $\boldsymbol{k} \to \infty$ were studied in detail in [20]. It was found there that requiring

$$\lim_{\boldsymbol{k}\to\infty} \frac{\mathfrak{w}}{\boldsymbol{k}}\bigg|_{[\text{scalar}]} \leq 1\,, \tag{3.1}$$

constraints λ_{GB} as follows

$$\lambda_{\text{GB}} \leq \lambda_{\text{GB}}^{\text{scalar}} = \frac{9}{100}\,. \tag{3.2}$$

Note that $\lambda_{\text{GB}}^{\text{scalar}} < \lambda_{\text{max}}$ found in the context of the second-order truncated hydrodynamics. In the remainder of this section we extend analysis of [19, 20] to the shear and the sound channel quasinormal modes.

3.1 Causality in the shear channel

It is straightforward to derive the shear channel quasinormal equation for the GB black holes:

$$Z''_{[\text{shear}]}(u) + \mathcal{C}^{(1)}_{\text{shear}}\; Z'_{[\text{shear}]}(u) + \mathcal{C}^{(2)}_{\text{shear}}\; Z_{[\text{shear}]}(u) = 0\,, \tag{3.3}$$

where the coefficients $\mathcal{C}^{(i)}_{\text{shear}}$ are presented in appendix B. Following [20], we now caste (3.3) into the form of the Schrödinger equation. Towards this end, we introduce a new radial coordinate y

$$\frac{dy}{du} = -\frac{1}{u^{1/2} f(u)}\,, \tag{3.4}$$

and rescale the radial profile as

$$Z_{[\text{shear}]} = \frac{1}{\mathcal{B}}\; \psi_{[\text{shear}]}\,, \tag{3.5}$$

with

$$\frac{d}{du}\ln\mathcal{B} = \Big(4u(2\lambda_{\rm GB}f-1)^2(\alpha^2(2\lambda_{\rm GB}f-1)^2+\mathcal{A}^2 f(4\lambda_{\rm GB}-1))\Big)^{-1} \times\Big(\mathcal{A}^2(1-4\lambda_{\rm GB})(12f^3\lambda_{\rm GB}^2-16f^2\lambda_{\rm GB}-4+7f)-(20f^2\lambda_{\rm GB}^2-20\lambda_{\rm GB}f +8\lambda_{\rm GB}+3)(2\lambda_{\rm GB}f-1)^2\alpha^2\Big)\,, \tag{3.6}$$

where $\alpha = \mathfrak{w}/\boldsymbol{k}$. The quasinormal equation (3.3) can then be rewritten as

$$-\hbar^2\,\partial_y^2\,\psi_{[\rm shear]}+U_{[\rm shear]}\;\psi_{[\rm shear]}=\alpha^2\;\psi_{[\rm shear]}\,,\qquad \hbar\equiv\frac{1}{\boldsymbol{k}}\,, \qquad \text{where}\quad U_{[\rm shear]}=U^0_{[\rm shear]}+\hbar^2\;U^1_{[\rm shear]}\,. \tag{3.7}$$

The first part of the effective potential has the simple form when expressed in terms of u

$$U^0_{[\rm shear]}(u) = \frac{f\mathcal{A}^2(1-4\lambda_{\rm GB})}{(2\lambda_{\rm GB}f-1)^2} = \frac{(1-4\lambda_{\rm GB})\,(1-\sqrt{1-4\lambda_{\rm GB}(1-u^2)})}{(1-4\lambda_{\rm GB}(1-u^2))\,(1-\sqrt{1-4\lambda_{\rm GB}})}\,, \tag{3.8}$$

while the expression for $U^1_{\rm shear}$ is too long to be presented here, but we note that the latter is a function only of u, $\lambda_{\rm GB}$ and α. What is important is that in the limit $\boldsymbol{k}\to\infty$ (or $\hbar\to 0$), everywhere except in the tiny region $y\gtrsim -\frac{1}{\boldsymbol{k}}$ the dominant contribution to $U_{\rm shear}$ comes from $U^0_{\rm shear}$. Thus in this limit we simply replace

$$\hbar^2\,U^1_{[\rm shear]}=\begin{cases}0 & y<0\,,\\ +\infty & y\geq 0\,.\end{cases} \tag{3.9}$$

Figure 3 illustrates the general behaviour of the leading potential (3.8). For any values of $\lambda_{\rm GB}$, we have in the asymptotic region, $U^0_{[\rm shear]}(u=0)=1$ while at the horizon, $U^0_{[\rm shear]}(u=1)=0$. Now for small values of $|\lambda_{\rm GB}|$, $U^0_{[\rm shear]}$ is a monotonically decreasing function between these two points. However, for larger negative values of $\lambda_{\rm GB}$, the potential develops a (single) maximum at intermediate value of u:

$$U^0_{\rm max}=\frac{1-4\lambda_{\rm GB}}{4(\sqrt{1-4\lambda_{\rm GB}}-1)} \qquad \text{at}\quad u_{\rm max}=-\frac{\sqrt{\lambda_{\rm GB}\,(3+4\lambda_{\rm GB})}}{2\lambda_{\rm GB}}\,. \tag{3.10}$$

As might be inferred from $u_{\rm max}$ above, the critical coupling for the appearance of this maximum is $\lambda_{\rm GB}=-3/4$. At this stage, the analysis is identical to that for the scalar channel studied in [20]. Once the effective potential in the Schrödinger problem (3.7) develops this new maximum, there always exist quasinormal modes with $\mathrm{Re}\,(\alpha^2)\simeq U^0_{\rm max}>1$. This implies then that in the limit of infinte $\boldsymbol{k}$, $\mathrm{Re}(\mathfrak{w})/\boldsymbol{k}>1$ for these modes and hence they lead to a violation of causality. Hence requiring the excitations in the shear channel to be well behaved imposes the constraint:

$$\lambda_{\rm GB}\geq\lambda_{\rm GB}^{\rm shear}=-\frac{3}{4}\,. \tag{3.11}$$

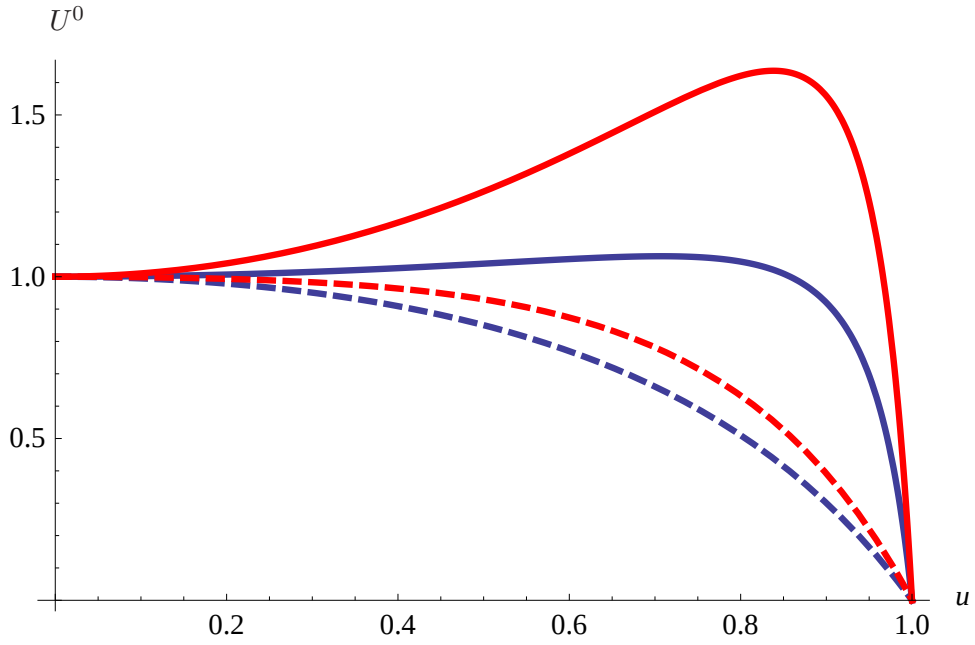

Figure 3. (Colour online) Typical behaviour of U^0, the leading contribution to the Schrödinger potential, for both the shear (blue) and sound (red) channels. The solid and dashed curves show the behaviour for large and small $|\lambda_{\rm GB}|$, respectively. (Our representative values here are: $\lambda_{\rm GB} = -1.5$ and -0.15.)

3.2 Causality in the sound channel

The quasinormal equation for the sound channel is given in (2.7). Following [20] (as reviewed in the previous section), we arrive at the corresponding Schrödinger problem in the sound channel

$$-\hbar^2\ \partial_y^2\,\psi_{[\rm sound]} + U_{[\rm sound]}\ \psi_{[\rm sound]} = \alpha^2\ \psi_{[\rm sound]}\,. \tag{3.12}$$

Once again, in the limit $\boldsymbol{k} \to \infty$, potential $U_{[\rm sound]}$ is given by

$$U_{[\rm sound]} = \begin{cases} U^0_{[\rm sound]} & y < 0\,, \\ +\infty & y = 0\,. \end{cases} \tag{3.13}$$

where

$$\begin{aligned} U^0_{[\rm sound]} &= \frac{(1 - 8\lambda_{\rm GB} - 4f\lambda_{\rm GB}(\lambda_{\rm GB} f - 1))A^2 f}{(2\lambda_{\rm GB} f - 1)^2} \\ &= \frac{(1 - 4\lambda_{\rm GB}(1+u^2))\,(1 - \sqrt{1 - 4\lambda_{\rm GB}(1-u^2)})}{(1 - 4\lambda_{\rm GB}(1-u^2))\,(1 - \sqrt{1 - 4\lambda_{\rm GB}})}\,. \end{aligned} \tag{3.14}$$

The general behaviour of this potential is the same as described in the previous section, as can be seen in figure 3. In particular, to avoid the appearance of an intermediate maximum in the potential (3.14) and the corresponding causality-violating quasinormal modes, we must impose the constraint

$$\lambda_{\rm GB} \geq \lambda_{\rm GB}^{\rm sound} = -\frac{7}{36}\,. \tag{3.15}$$

JHEP08(2009)016

Note that $\lambda_{\rm GB}^{\rm sound} > \lambda_{\rm GB}^{\rm shear}$ found above and also $\lambda_{\rm GB}^{\rm sound} > \lambda_{\rm min}$ found in the context of the second-order truncated hydrodynamics.

4 Conclusion

In this paper, we have shown how causality of the near-equilibrium phenomena in the quantum field theory can be used to distinguish "healthy" models from the "sick" ones. To illustrate the point, we studied the fluctuations in the CFT plasmas, holographically dual to Gauss-Bonnet gravity (1.12). Our analysis found two sets of constraints on the GB coupling:

$$\text{second-order hydrodynamics: } -0.711 \leq \lambda_{\rm GB} \leq 0.113\,, \tag{4.1}$$

$$\text{exact analysis: } \quad -\tfrac{7}{36} \leq \lambda_{\rm GB} \leq \tfrac{9}{100}\ . \tag{4.2}$$

It is clear that the exact analysis of section 3 produced more stringent restrictions than the analysis of the truncated second-order hydrodynamic equations in section 2. While both of these approaches are examining the behaviour of gravitational fluctuations in the GB black hole background (2.3), the relevant quasinormal modes are very different in the two cases. The second-order hydrodynamics is focussed entirely on the behaviour of the sound mode, i.e., the lowest quasinormal mode in the sound channel. In contrast, the potential causality violation by highly excited quasinormal modes in the scalar channel set the upper bound in (4.2) while the lower bound arises from a similar set of quasinormal modes in the sound channel.

We must emphasize that the status of these constraints differs at a very basic level. Theories outside of the bounds given in (4.2) are fundamentally pathological. In contrast, the constraints (4.1) simply indicate where a certain approximate description of the fluid becomes problematic. As such, it is somewhat remarkable then that the bounds coming from these two very different approaches seem to be fairly close to each other. It is also satisfying that the fundamental constraints (4.2) are the most restrictive so that the truncated second-order hydrodynamics will be stable in any of the cases where the underlying theory is physically sound at a fundamental level. A priori, this does not seem to be required by any basic principles.

We consider the second-order hydrodynamics and the behaviour of the lowest sound quasinormal mode in more detail in figures 4 and 5, which show results for $\lambda_{\rm GB} = -2.5$ — note that the latter is outside the "healthy" ranges in both (4.1) and (4.2). Using the truncated second-order equations only yields physically reliable results for $\boldsymbol{k} \ll 1$, where the dispersion relation can be Taylor-expanded as in (2.1). These Taylor expansions for the phase velocity and the width, i.e., $\mathrm{Re}(\mathfrak{w})/\boldsymbol{k}$ and $\mathrm{Im}(\mathfrak{w})$, keeping only the $O(\boldsymbol{k}^2)$ terms are illustrated with the green curves in the two figures. On the other hand, the causality analysis of section 2 treats the dispersion relation (1.9) as exact and the results are shown with the red curves. In this case as $\boldsymbol{k} \to \infty$, the phase velocity rises to $\mathrm{Re}(\mathfrak{w})/\boldsymbol{k} = v_{[\rm sound]}^{\rm front} \simeq 1.126$ and the width also reaches a finite value asymptotically

$$\lim_{|\boldsymbol{k}|\to\infty} \left.\frac{\mathrm{Im}\,(\mathfrak{w})}{\boldsymbol{k}}\right|_{[\rm sound]} = -\frac{1}{\pi\,\tau_\Pi T}\,\frac{\eta/s}{\tau_\Pi T + 4\,\eta/s} \simeq -0.047\,. \tag{4.3}$$

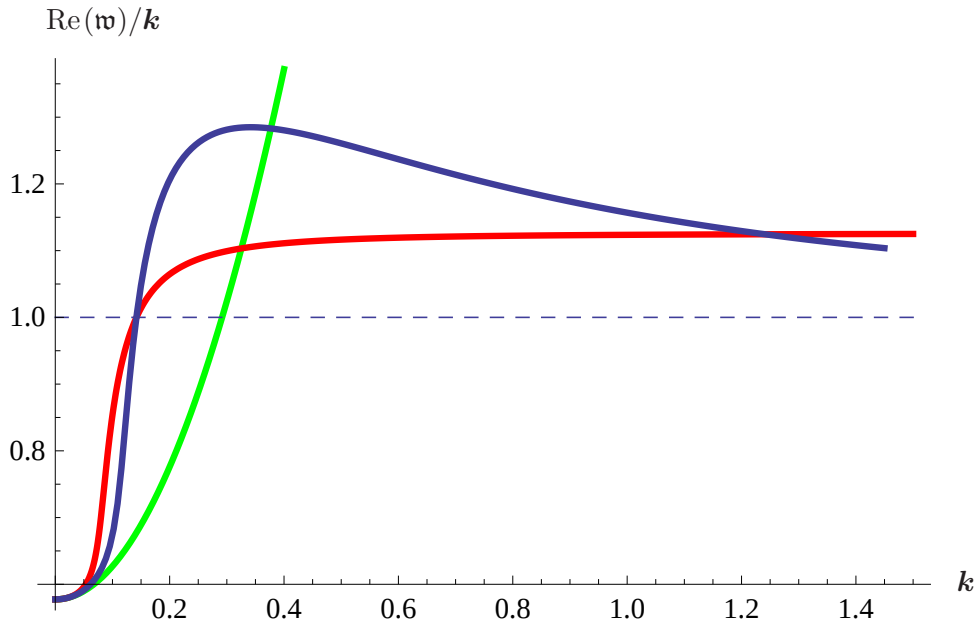

Figure 4. (Colour online) The phase velocity $\mathrm{Re}(\mathfrak{w})/\boldsymbol{k}$ for $\lambda_{\mathrm{GB}} = -2.5$: The blue line shows the behaviour of the lowest quasinormal mode calculated numerically. The red curve corresponds the second-order hydrodynamic approximation (1.9). The green curve corresponds the next order Taylor expansion (2.1) arising from the second-order dispersion relation.

As is evident in the figures, these "exact" dispersion relations only match the Taylor expansion (2.1) for small values of $\boldsymbol{k}$.[5]

To emphasize the limitations of treating (1.9) as an "exact" dispersion relation, figures 4 and 5 also show numerical results for the behavior of the sound mode, i.e., the lowest quasinormal mode with the blue curves. As expected, all of the different curves agree at small $\boldsymbol{k}$ but not at large $\boldsymbol{k}$. While not unexpected, we wish, in particular, to point out that the striking differences between the actual behaviour of the sound mode and the second-order hydrodynamic dispersion relation (1.9). Figure 5 shows that the actual width decays rapidly to zero in contrast to the finite asymptotic limit, given in (4.3) above, for the second-order dispersion relation. Similarly in figure 4, the actual phase velocity rises beyond $v^{\mathrm{front}}_{[\mathrm{sound}]} \simeq 1.126$, the asymptotic limit found for second-order hydrodynamics, but then appears to decay back towards one as $\boldsymbol{k} \to \infty$. While the numerical results shown are already becoming less reliable for $\boldsymbol{k} > 1$,[6] it seems that the limit $\boldsymbol{k} \to \infty$ should produce a front velocity which respects causality.[7]

Despite the fact that the results of (1.9) may have little resemblance to the physical behaviour of the sound mode at large $\boldsymbol{k}$, it remains important that the truncated second-order

[5] In fact, it may seem that, in figures 4 and 5, the two sets of curves begin to separate at surprisingly small wave numbers (i.e., $\boldsymbol{k} \sim 0.05$ to 0.10). This observation can be explained by examining the Taylor series to higher orders. We find roughly an expansion in $[(1-4\lambda_{\mathrm{GB}})^2\boldsymbol{k}^2]^n$ for large λ_{GB} and so with $\lambda_{\mathrm{GB}} = -2.5$, the Taylor series should only be expected to match the "exact" result for $\boldsymbol{k} \ll 1/11$.

[6] These numerical difficulties are correlated to the dramatic decrease in $|\mathrm{Im}(\mathfrak{w})|$.

[7] Of course, the higher quasinormal modes are expected to violate causality with $v_{\mathrm{max}} \simeq 1.415$, using the analysis of the effective Schrödinger potential (3.14).

JHEP08(2009)016

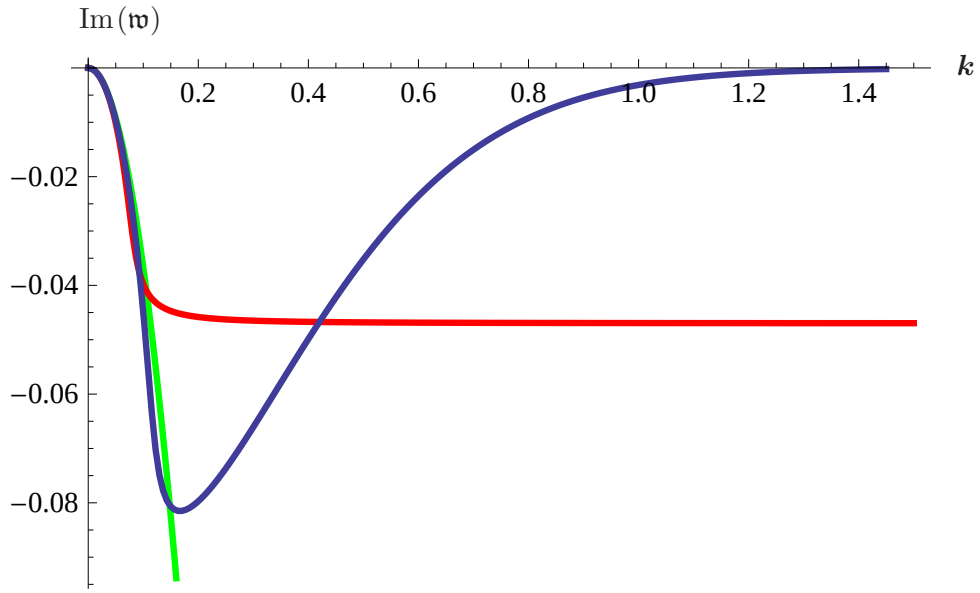

Figure 5. (Colour online) The decay width $\mathrm{Im}(\varpi)$ for $\lambda_{\rm GB} = -2.5$: The blue line shows the behaviour of the lowest quasinormal mode calculated numerically. The red curve corresponds the second-order hydrodynamic approximation (1.9). The green curve corresponds the next order Taylor expansion (2.1) arising from the second-order dispersion relation.

hydrodynamic equations present a robust mathematical framework in certain situations. For example, numerical simulations of the strongly coupled quark-gluon plasma [6] implicitly extrapolate the hydrodynamic equations to the smallest numerical scales, even though the physics of interest is in the hydrodynamic regime. In this situation, having a system of hyperbolic equations which is causal is of course essential.

Our holographic construction with Gauss-Bonnet gravity provides a simple toy model in which the dual CFT is completely specified by two central charges c and a. The exact relation of these CFT parameters to the gravitational couplings in the action (1.12) is given by [16, 25]

$$\begin{aligned} c &= \frac{\pi^2}{2^{3/2}}\frac{L^3}{\ell_P^3}\,(1+\sqrt{1-4\lambda_{\rm GB}})^{3/2}\,\sqrt{1-4\lambda_{\rm GB}}\,, \\ a &= \frac{\pi^2}{2^{3/2}}\frac{L^3}{\ell_P^3}\,(1+\sqrt{1-4\lambda_{\rm GB}})^{3/2}\,\left(3\sqrt{1-4\lambda_{\rm GB}}-2\right)\,, \end{aligned} \tag{4.4}$$

and hence

$$\frac{c-a}{c} = 2\left(\frac{1}{\sqrt{1-4\lambda_{\rm GB}}}-1\right)\,. \tag{4.5}$$

As $\lambda_{\rm GB}$ alone fixes this last combination, we may re-express our causality constraints (4.2) in terms of the central charges, which yields the elegant result:

$$-\frac{1}{2} \le \frac{c-a}{c} \le \frac{1}{2}\,. \tag{4.6}$$

Here we have focussed on the fundamental constraint (4.2) rather than the second-order hydrodynamic constraint (4.1) and have found that if the difference in the central charges

grows too large, some linearized fluctuations in the model propagate faster than the speed of light.

These constraints are also intriguing in comparison to the analysis of four-dimensional CFT's presented by Hofman and Maldacena [26]. They consider "experiments" in which the energy flux was measured in various directions at null infinity after a local disturbance was created in the stress energy. This energy flux was found to be controlled by the three-point function of the stress tensor in the CFT. Further it was shown that the parameters fixing this three-point function must be constrained in order that the energy flux was always positive. The holographic dual describing this CFT "experiment" would involve both curvature-squared and curvature-cubed interactions. However, if the CFT was restricted so as to eliminate the curvature-cubed interaction in the gravitational dual,[8] then the positive energy constraint reduced to a constraint on the central charges, which in fact precisely matches that given in (4.6). The precise agreement of the upper bound was already noted in [26].

One can go further in that measurements in the above "experiment" can be organized into three different channels, just as for the graviton fluctuations in section 3. With this classification, the upper bound in (4.6) comes from the appearance of negative energy flux in the scalar channel in [26] while it arises from causality violation in the same set of fluctuations in the holographic calculations [20]. Similarly, the lower bound is set to avoid problematic behaviour in the sound channel in both approaches. Then we may also note that while it did not set a fundamental constraint, causality violations also appear in the shear channel at the critical value given in (3.11): $\lambda_{\rm GB}^{\rm shear} = -\frac{3}{4}$. This result then translates to a critical value $(c-a)/c|_{\rm shear} = -1$, which again precisely matches that for the appearance of negative energy fluxes in the shear channel. Hence, at least within this holographic model, we have drawn a precise correlation between the appearance of negative energy fluxes and of superluminal signals in various channels.

We close with a few comments about other potential instabilities in this holographic model. It was observed in [19] that a new instability arises in the dual plasma at $\lambda_{\rm GB} = -1/8$. At this point, the effective Schrödinger potential develops a small well where $U^0 < 0$ just in front of the horizon (i.e., near $u = 1$). For sufficiently large $\boldsymbol{k}$ (and $|\lambda_{\rm GB}|$), this well will support unstable quasinormal modes, as described in [27].[9] Examining (3.14) reveals similar behaviour and hence instabilities for $\lambda_{\rm GB} > 1/8$ in the sound channel, however, this problem only appears outside of the range (4.2) allowed by causality. Formally, the effective potential (3.8) in the shear channel shows a similar behaviour for $\lambda_{\rm GB} > 1/4$ but this is again of no consequence since, as noted before, our entire analysis is only valid in the regime $\lambda_{\rm GB} < 1/4$. Hence the instability in the scalar channel is the only one that appears within the physical regime (4.2). This instability does not correspond to a fundamental pathology with the theory but rather indicates that the uniform plasma becomes unstable with respect to certain non-uniform perturbations. It would of course be interesting to follow the full nonlinear effect of these instabilities. On the gravitational

[8] This restriction would be realized in any supersymmetric CFT.

[9] It was later observed that this instability seems to be increased by a chemical potential [28].

JHEP08(2009)016

side, this instability seems similar in certain respects to the Gregory-Laflamme instability for black strings [29].

Acknowledgments

After this work was finished, we became aware of an upcoming paper [30] which has significant overlap with sections 3 and 4. We would like to thank Diego Hofman for sharing an early draft of [30] with us. It is also a pleasure to thank Karl Landsteiner, Paul Romatschke, Aninda Sinha and Andrei Starinets for useful correspondence and conversations. Research at Perimeter Institute is supported by the Government of Canada through Industry Canada and by the Province of Ontario through the Ministry of Research & Innovation. AB gratefully acknowledges further support by an NSERC Discovery grant and support through the Early Researcher Award program by the Province of Ontario. RCM also acknowledges support from an NSERC Discovery grant and funding from the Canadian Institute for Advanced Research.

A Coefficients of (2.7)

$$
\begin{aligned}
\mathcal{C}^{(1)}_{\text{sound}} = &\Big(fu\,(f\mathcal{A}^2\boldsymbol{k}^2+2\mathcal{A}^2\boldsymbol{k}^2-3\mathfrak{w}^2)-2f^2u\,(f\mathcal{A}^2\boldsymbol{k}^2+10\mathcal{A}^2\boldsymbol{k}^2-12\mathfrak{w}^2)\lambda_{\text{GB}}\\
&-4f^3u\,(f\mathcal{A}^2\boldsymbol{k}^2-14\mathcal{A}^2\boldsymbol{k}^2+18\mathfrak{w}^2)\lambda^2_{\text{GB}}+8f^4u\,(f\mathcal{A}^2\boldsymbol{k}^2-6\mathcal{A}^2\boldsymbol{k}^2+12\mathfrak{w}^2)\lambda^3_{\text{GB}}\\
&-48f^5u\,\mathfrak{w}^2\lambda^4_{\text{GB}}\Big)^{-1}\times\Big(-4\mathcal{A}^2\boldsymbol{k}^2+6\mathfrak{w}^2-3f\mathfrak{w}^2+4f\mathcal{A}^2\boldsymbol{k}^2-3f^2\mathcal{A}^2\boldsymbol{k}^2\\
&-2f(12\mathfrak{w}^2-3f\mathfrak{w}^2+8f^2\mathcal{A}^2\boldsymbol{k}^2-4\mathcal{A}^2\boldsymbol{k}^2-14f\mathcal{A}^2\boldsymbol{k}^2)\lambda_{\text{GB}}+24f^2(-4\mathcal{A}^2\boldsymbol{k}^2\\
&+f\mathfrak{w}^2+\mathfrak{w}^2+f^2\mathcal{A}^2\boldsymbol{k}^2+2f\mathcal{A}^2\boldsymbol{k}^2)\lambda^2_{\text{GB}}-8f^4(f\mathcal{A}^2\boldsymbol{k}^2+6\mathcal{A}^2\boldsymbol{k}^2+9\mathfrak{w}^2)\lambda^3_{\text{GB}}\\
&+48f^5\lambda^4_{\text{GB}}\mathfrak{w}^2\Big)
\end{aligned}
\tag{A.1}
$$

$$
\begin{aligned}
\mathcal{C}^{(2)}_{\text{sound}} = &\Big(f^2u^2\left[-(f\mathcal{A}^2\boldsymbol{k}^2+2\mathcal{A}^2\boldsymbol{k}^2-3\mathfrak{w}^2)+2f(12\mathcal{A}^2\boldsymbol{k}^2+2f\mathcal{A}^2\boldsymbol{k}^2-15\mathfrak{w}^2)\lambda_{\text{GB}}\right.\\
&-24f^2(-5\mathfrak{w}^2+4\mathcal{A}^2\boldsymbol{k}^2)\lambda^2_{\text{GB}}-16f^3(15\mathfrak{w}^2-10\mathcal{A}^2\boldsymbol{k}^2+f\mathcal{A}^2\boldsymbol{k}^2)\lambda^3_{\text{GB}}\\
&\left.+16f^4(15\mathfrak{w}^2-6\mathcal{A}^2\boldsymbol{k}^2+f\mathcal{A}^2\boldsymbol{k}^2)\lambda^4_{\text{GB}}-96f^5\mathfrak{w}^2\lambda^5_{\text{GB}}\right]\Big)^{-1}\times\Big(3\mathfrak{w}^4u-4f\mathcal{A}^2\boldsymbol{k}^2\\
&+f^2\mathcal{A}^4\boldsymbol{k}^4u+8f^2\mathcal{A}^2\boldsymbol{k}^2-4f^3\mathcal{A}^2\boldsymbol{k}^2-4\mathfrak{w}^2f\mathcal{A}^2\boldsymbol{k}^2u-2\mathfrak{w}^2\mathcal{A}^2\boldsymbol{k}^2u+2\mathcal{A}^4\boldsymbol{k}^4fu\\
&+2f(5f\mathfrak{w}^2u\mathcal{A}^2\boldsymbol{k}^2-8f^3\mathcal{A}^2\boldsymbol{k}^2-15\mathfrak{w}^4u-28f\mathcal{A}^2\boldsymbol{k}^2-8\mathcal{A}^4\boldsymbol{k}^4u+8\mathcal{A}^2\boldsymbol{k}^2\\
&+2f^2\mathcal{A}^4\boldsymbol{k}^4u+24\mathfrak{w}^2\mathcal{A}^2\boldsymbol{k}^2u-8f\mathcal{A}^4\boldsymbol{k}^4u+28f^2\mathcal{A}^2\boldsymbol{k}^2)\lambda_{\text{GB}}-4f^2(-30\mathfrak{w}^4u\\
&-12f\mathfrak{w}^2u\mathcal{A}^2\boldsymbol{k}^2-32\mathcal{A}^4\boldsymbol{k}^4u-4f^2\mathcal{A}^2\boldsymbol{k}^2+2f^2\mathcal{A}^4\boldsymbol{k}^4u+12f\mathcal{A}^4\boldsymbol{k}^4u+40f\mathcal{A}^2\boldsymbol{k}^2\\
&+60\mathfrak{w}^2\mathcal{A}^2\boldsymbol{k}^2u-24\mathcal{A}^2\boldsymbol{k}^2-11f^3\mathcal{A}^2\boldsymbol{k}^2)\lambda^2_{\text{GB}}-8f^3(2f^2\mathcal{A}^4\boldsymbol{k}^4u-56\mathfrak{w}^2\mathcal{A}^2\boldsymbol{k}^2u\\
&+3f^3\mathcal{A}^2\boldsymbol{k}^2-24\mathcal{A}^4\boldsymbol{k}^4fu+22f^2\mathcal{A}^2\boldsymbol{k}^2+26\mathfrak{w}^2f\mathcal{A}^2\boldsymbol{k}^2u-24f\mathcal{A}^2\boldsymbol{k}^2+30\mathfrak{w}^4u\\
&+24\mathcal{A}^4\boldsymbol{k}^4u)\lambda^3_{\text{GB}}+16f^4(16\mathfrak{w}^2f\mathcal{A}^2\boldsymbol{k}^2u-18\mathfrak{w}^2\mathcal{A}^2\boldsymbol{k}^2u-6\mathcal{A}^4\boldsymbol{k}^4fu+6f^2\mathcal{A}^2\boldsymbol{k}^2\\
&+f^2\mathcal{A}^4\boldsymbol{k}^4u+15\mathfrak{w}^4u)\lambda^4_{\text{GB}}-96f^5u\,\mathfrak{w}^2(\mathfrak{w}^2+f\mathcal{A}^2\boldsymbol{k}^2)\lambda^5_{\text{GB}}\Big)
\end{aligned}
\tag{A.2}
$$

where f is given by (2.4).

JHEP08(2009)016

B Coefficients of (3.3)

$$\mathcal{C}^{(1)}_{\rm shear} = \Big(-fu\,(-\mathfrak{w}^2+f\mathcal{A}^2\boldsymbol{k}^2)+4f^2u\,(f\mathcal{A}^2\boldsymbol{k}^2-2\mathfrak{w}^2+\boldsymbol{k}^2\mathcal{A}^2)\lambda_{\rm GB}$$
$$-4f^3u(f\mathcal{A}^2\boldsymbol{k}^2-6\mathfrak{w}^2+4\boldsymbol{k}^2\mathcal{A}^2)\lambda^2_{\rm GB}+16f^4u(-2\mathfrak{w}^2+\mathcal{A}^2\boldsymbol{k}^2)\lambda^3_{\rm GB}+16f^5u\,\mathfrak{w}^2\lambda^4_{\rm GB}\Big)^{-1}$$
$$\times\Big(f^2\mathcal{A}^2\boldsymbol{k}^2-2\mathfrak{w}^2+f\mathfrak{w}^2-2f(4f\mathcal{A}^2\boldsymbol{k}^2+f\mathfrak{w}^2-4\mathfrak{w}^2)\lambda_{\rm GB}+8f^2(-f\mathfrak{w}^2-\mathfrak{w}^2$$
$$+2\boldsymbol{k}^2\mathcal{A}^2)\lambda^2_{\rm GB}+24f^4\lambda^3_{\rm GB}\mathfrak{w}^2-16f^5\lambda^4_{\rm GB}\mathfrak{w}^2\Big) \tag{B.1}$$

$$\mathcal{C}^{(2)}_{\rm shear} = \Big((2\lambda_{\rm GB}f-1)^2f^2u\Big)^{-1}\times\Big(\mathfrak{w}^2-f\mathcal{A}^2\boldsymbol{k}^2+4f(\boldsymbol{k}^2\mathcal{A}^2-\mathfrak{w}^2)\lambda_{\rm GB}+4f^2\lambda^2_{\rm GB}\mathfrak{w}^2\Big) \tag{B.2}$$

where f is given by (2.4).

References

[1] P. Romatschke, *Relativistic viscous fluid dynamics and non-equilibrium entropy*, arXiv:0906.4787 [SPIRES].

[2] R. Baier, P. Romatschke, D.T. Son, A.O. Starinets and M.A. Stephanov, *Relativistic viscous hydrodynamics, conformal invariance and holography*, *JHEP* **04** (2008) 100 [arXiv:0712.2451] [SPIRES].

[3] I. Müller, *Zum Paradoxon der Wärmeleitungstheorie*, *Z. Phys.* **198** (1967) 329;
W. Israel, *Nonstationary irreversible thermodynamics: a causal relativistic theory*, *Ann. Phys.* **100** (1976) 310 [SPIRES];
W. Israel and J.M. Stewart, *Thermodynamics of nonstationary and transient effects in a relativistic gas*, *Phys. Lett.* **A 58** (1976) 213; *Transient relativistic thermodynamics and kinetic theory*, *Ann. Phys.* **118** (1979) 341 [SPIRES].

[4] W.A. Hiscock and L. Lindblom, *Stability and causality in dissipative relativistic fluids*, *Annals Phys.* **151** (1983) 466 [SPIRES]; *Linear plane waves in dissipative relativistic fluids*, *Phys. Rev.* **D 35** (1987) 3723 [SPIRES]; *Generic instabilities in first-order dissiPative relativistic fluid theories*, *Phys. Rev.* **D 31** (1985) 725 [SPIRES].

[5] A. Muronga, *Causal theories of dissipative relativistic fluid dynamics for nuclear collisions*, *Phys. Rev.* **C 69** (2004) 034903 [nucl-th/0309055] [SPIRES].

[6] See, for example H. Song and U.W. Heinz, *Extracting the QGP viscosity from RHIC data — A status report from viscous hydrodynamics*, arXiv:0812.4274 [SPIRES];
M. Luzum and P. Romatschke, *Conformal relativistic viscous hydrodynamics: applications to RHIC results at* $\sqrt{s_{NN}} = 200\,GeV$, *Phys. Rev.* **C 78** (2008) 034915 [*Erratum ibid.* **C 79** (2009) 039903] [arXiv:0804.4015] [SPIRES].

[7] See, for example, L. Brillouin, *Wave propagation and group velocity*, Academic Press, New York U.S.A. (1960);
R. Fox, C.G. Kuper and S.G. Lipson, *Faster-than-light group velocities and causality violation*, *Proc. Roy. Soc. Lond.* **A 316** (1970) 515 [SPIRES];
E. Krotscheck and W. Kundt, *Causality criteria*, *Commun. Math. Phys.* **60** (1978) 171.

[8] P. Romatschke, *New developments in relativistic viscous hydrodynamics*, arXiv:0902.3663 [SPIRES].

JHEP08(2009)016

[9] J.M. Maldacena, *The large-N limit of superconformal field theories and supergravity*, *Adv. Theor. Math. Phys.* **2** (1998) 231 [*Int. J. Theor. Phys.* **38** (1999) 1113] [hep-th/9711200] [SPIRES].

[10] O. Aharony, S.S. Gubser, J.M. Maldacena, H. Ooguri and Y. Oz, *Large-N field theories, string theory and gravity*, *Phys. Rept.* **323** (2000) 183 [hep-th/9905111] [SPIRES].

[11] S. Bhattacharyya, V.E. Hubeny, S. Minwalla and M. Rangamani, *Nonlinear fluid dynamics from gravity*, *JHEP* **02** (2008) 045 [arXiv:0712.2456] [SPIRES].

[12] D.T. Son and A.O. Starinets, *Viscosity, black holes and quantum field theory*, *Ann. Rev. Nucl. Part. Sci.* **57** (2007) 95 [arXiv:0704.0240] [SPIRES].

[13] G. Policastro, D.T. Son and A.O. Starinets, *The shear viscosity of strongly coupled $N = 4$ supersymmetric Yang-Mills plasma*, *Phys. Rev. Lett.* **87** (2001) 081601 [hep-th/0104066] [SPIRES].

[14] R.C. Myers, M.F. Paulos and A. Sinha, *Quantum corrections to η_s*, *Phys. Rev.* **D 79** (2009) 041901 [arXiv:0806.2156] [SPIRES];
A. Buchel, R.C. Myers, M.F. Paulos and A. Sinha, *Universal holographic hydrodynamics at finite coupling*, *Phys. Lett.* **B 669** (2008) 364 [arXiv:0808.1837] [SPIRES].

[15] I. Amado, C. Hoyos-Badajoz, K. Landsteiner and S. Montero, *Hydrodynamics and beyond in the strongly coupled $N = 4$ plasma*, *JHEP* (2008) 133 [arXiv:0805.2570] [SPIRES].

[16] S. Nojiri and S.D. Odintsov, *On the conformal anomaly from higher derivative gravity in AdS/CFT correspondence*, *Int. J. Mod. Phys.* **A 15** (2000) 413 [hep-th/9903033] [SPIRES].

[17] M. Blau, K.S. Narain and E. Gava, *On subleading contributions to the AdS/CFT trace anomaly*, *JHEP* **09** (1999) 018 [hep-th/9904179] [SPIRES].

[18] Y. Kats and P. Petrov, *Effect of curvature squared corrections in AdS on the viscosity of the dual gauge theory*, *JHEP* **01** (2009) 044 [arXiv:0712.0743] [SPIRES];
A. Buchel, R.C. Myers and A. Sinha, *Beyond $\eta_s = 1/4\pi$*, *JHEP* **03** (2009) 084 [arXiv:0812.2521] [SPIRES].

[19] M. Brigante, H. Liu, R.C. Myers, S. Shenker and S. Yaida, *Viscosity bound violation in higher derivative gravity*, *Phys. Rev.* **D 77** (2008) 126006 [arXiv:0712.0805] [SPIRES].

[20] M. Brigante, H. Liu, R.C. Myers, S. Shenker and S. Yaida, *The viscosity bound and causality violation*, *Phys. Rev. Lett.* **100** (2008) 191601 [arXiv:0802.3318] [SPIRES].

[21] P.K. Kovtun and A.O. Starinets, *Quasinormal modes and holography*, *Phys. Rev.* **D 72** (2005) 086009 [hep-th/0506184] [SPIRES].

[22] R.-G. Cai, *Gauss-Bonnet black holes in AdS spaces*, *Phys. Rev.* **D 65** (2002) 084014 [hep-th/0109133] [SPIRES].

[23] S. Nojiri and S.D. Odintsov, *Anti-de Sitter black hole thermodynamics in higher derivative gravity and new confining-deconfining phases in dual CFT*, *Phys. Lett.* **B 521** (2001) 87 [*Erratum ibid.* **B 542** (2002) 301] [hep-th/0109122] [SPIRES];
Y.M. Cho and I.P. Neupane, *Anti-de Sitter black holes, thermal phase transition and holography in higher curvature gravity*, *Phys. Rev.* **D 66** (2002) 024044 [hep-th/0202140] [SPIRES];
I.P. Neupane, *Black hole entropy in string-generated gravity models*, *Phys. Rev.* **D 67** (2003) 061501 [hep-th/0212092] [SPIRES]; *Thermodynamic and gravitational instability on hyperbolic spaces*, *Phys. Rev.* **D 69** (2004) 084011 [hep-th/0302132] [SPIRES].

JHEP08(2009)016

[24] G. Policastro, D.T. Son and A.O. Starinets, *From AdS/CFT correspondence to hydrodynamics*, *JHEP* **09** (2002) 043 [hep-th/0205052] [SPIRES].

[25] R.C. Myers, M.F. Paulos and A. Sinha, in preparation.

[26] D.M. Hofman and J. Maldacena, *Conformal collider physics: energy and charge correlations*, *JHEP* **05** (2008) 012 [arXiv:0803.1467] [SPIRES].

[27] R.C. Myers, A.O. Starinets and R.M. Thomson, *Holographic spectral functions and diffusion constants for fundamental matter*, *JHEP* **11** (2007) 091 [arXiv:0706.0162] [SPIRES].

[28] X.-H. Ge, Y. Matsuo, F.-W. Shu, S.-J. Sin and T. Tsukioka, *Viscosity bound, causality violation and instability with stringy correction and charge*, *JHEP* **10** (2008) 009 [arXiv:0808.2354] [SPIRES].

[29] R. Gregory and R. Laflamme, *Black strings and p-branes are unstable*, *Phys. Rev. Lett.* **70** (1993) 2837 [hep-th/9301052] [SPIRES].

[30] D.M. Hofman and J. Maldacena, *Causality in higher derivative gravity and positivity of energy in a UV Complete QFT*, arXiv:0907.1625 [SPIRES].

JHEP08(2009)016